



Chemical and spatial analysis of protein loaded PLGA microspheres for drug delivery applications

A. Rafati^a, A. Boussahel^b, K.M. Shakesheff^b, A.G. Shard^c, C.J. Roberts^a, X. Chen^a, D.J. Scurr^a, S. Rigby-Singleton^d, P. Whiteside^d, M.R. Alexander^a, M.C. Davies^{a,*}

^a Laboratory of Biophysics and Surface Analysis, University of Nottingham, Nottinghamshire, NG7 2RD, UK

^b Centre for Biomedical Science, University of Nottingham, Nottinghamshire, NG7 2RD, UK

^c National Physical Laboratory, Teddington, London, TW11 0LW, UK

^d Molecular Profiles Ltd. Nottingham, Nottinghamshire, NG8 6PX, UK

ARTICLE INFO

Article history:

Received 31 January 2012

Accepted 1 May 2012

Available online 11 May 2012

Keywords:

Surface analysis

ToF-SIMS

Confocal Raman

Microsphere

Protein

Surfactant

ABSTRACT

Polymer microspheres for controlled release of therapeutic protein from within an implantable scaffold were produced and analysed using complimentary techniques to probe the surface and bulk chemistry of the microspheres. Time of Flight – Secondary Ion Mass Spectrometry (ToF-SIMS) surface analysis revealed a thin discontinuous film of polyvinyl alcohol (PVA) surfactant (circa 4.5 nm thick) at the surface which was readily removed under sputtering with C₆₀. Atomic Force Microscopy (AFM) imaging of microspheres before and after sputtering confirmed that the PVA layer was removed after sputtering revealing poly(lactic-co-glycolic) acid (PLGA). Scanning electron microscopy showed the spheres to be smooth with some shallow and generally circular depressions, often with pores in their central region. The occurrence of the protein at the surface was limited to areas surrounding these surface pores. This surface protein distribution is believed to be related to a burst release of the protein on dissolution. Analysis of the bulk properties of the microspheres by confocal Raman mapping revealed the 3D distribution of the protein showing large voids within the pores. Protein was found to be adsorbed at the interface with the PLGA oil phase following deposition on evaporation of the solvent. Protein was also observed concentrated within pores measuring approximately 2 µm across. The presence of protein in large voids and concentrated pores was further scrutinised by ToF-SIMS of sectioned microspheres. This paper demonstrates that important information for optimisation of such complex bioformulations, including an understanding of the release profile can be revealed by complementary surface and bulk analysis allowing optimisation of the therapeutic effect of such formulations.

© 2012 Published by Elsevier B.V.

1. Introduction

In recent years there has been an increase in the availability and development of protein and peptide controlled release therapeutics, such as microspheres for sustained perenteral delivery [1–5]. Applications of such systems include vaccination [2,6–8] and drug delivery [9–13], for periods of up to 6 months. Understanding the surface and the bulk chemical composition of such microspheres can provide significant insight into the production process and may also contribute to an understanding of the involvement of micro and nanostructure in drug release.

The work presented is concerned with a thorough physical and chemical characterisation of both the surface and bulk of a protein loaded PLGA microsphere formulation with a range of complementary techniques. The technique of Time of Flight – Secondary Ion Mass Spectrometry (ToF-SIMS) has been extensively used to study

pharmaceutical systems [14–19]. The utility of ToF-SIMS arises from the ability to provide high specificity chemical information with good depth resolution (~1–2 nm). Atomic Force Microscopy (AFM) is a complementary technique to ToF-SIMS providing nanometre spatial resolution of the surface topography which has been previously been applied to microsphere systems [20,21] for surface topography characterisation.

ToF-SIMS depth profiling has been used to analyse biomedically relevant thin films [17,19] to elucidate the spatial distribution of various constituents within such systems through the bulk of the sample. Due to the topography encountered with microsphere structure and the artefacts this can induce in ToF-SIMS data, this has not been as widely applied to the study of this type of structure. This is especially true for dual beam depth profiling whereby the sputter and analysis beams are often mounted 180° from one another (when viewed vertically above the microsphere) with each ion beam at a 45° elevation. Dual beam depth profiling therefore necessitates sample stage rotation and realignment of the sample stage between cycles of sputtering and analysis, in order to have both the sputter and analysis beam focussed on the same analysis region of the microsphere.

* Corresponding author. Tel.: +44 115 951 5063; fax: +44 115 846 7696.

E-mail address: martyn.davies@nottingham.ac.uk (M.C. Davies).

The analysis of the bulk of a formulation is crucial to the characterisation of pharmaceutical microsphere systems as the distribution of drug within the microsphere will significantly influence the release characteristics. Confocal Raman microscopy whereby a plane within a transparent sample is focussed on, and Raman spectra mapped for that focal plane providing a $\sim 1\ \mu\text{m}$ depth resolution was used for non-destructive bulk characterisation. It has been used in conjunction with ToF-SIMS of sectioned microspheres in this work in order to characterise the bulk distribution of the protein and the polymer. The results of this characterisation should allow for the distribution of constituent chemistries to be related back to the production process. Raman mapping has previously been applied to pharmaceutical systems including drug loaded polymeric microspheres [22,23], thin polymer films [18,19,24,25] and tablet compound identification [26], specifically using multivariate methods of analysis [27–29].

The use of these techniques (see Fig. 1) in combination allows for a 3D microscale characterisation of the drug delivery formulation and serves to illustrate the complementary use of surface analytical techniques for full characterisation of a PLGA microsphere drug delivery system. A double emulsion solvent evaporation process was used to produce the microspheres used in this study but any method of production is suitable for this approach. The protein lysozyme was used as a model protein therapeutic for release from the PLGA microspheres. This model was produced and characterised for fabricated microspheres that may be incorporated within a tissue engineering scaffold for bone repair providing mechanical support at the site of non-unified bone fractures [30,31]. Microspheres embedded within such a scaffold system have been shown to release therapeutic proteins, such as BMP2 to stimulate osteogenesis [32]. As the scaffold and microspheres degrade the protein therapeutic having stimulated bone repair will gradually transfer the load on the fracture from the scaffold to the new bone. It is hence crucial to characterise the composition of the protein loaded polymer microspheres to understand their performance in such a complex scaffold therapeutic system.

2. Materials and methods

Custom polymerised PLGA (56 kDa) was obtained from Lakeshore Biomaterials (Birmingham, Alabama, USA) consisting of 85:15 of DL-lactic acid and glycolic acid respectively. Polyvinyl alcohol (87–89%

hydrolysed) (PVA) and hen egg white lysozyme were purchased from Sigma Aldrich (Dorset, UK). The microspheres were produced using a water in oil in water double emulsion method containing 1.5%, 3%, 5% and 10% lysozyme as described in previous work [33,34].

ToF-SIMS data was acquired using a ToF-SIMS IV (ION-TOF GmbH, Munster, Germany) described elsewhere [35]. The samples were loaded by sprinkling on double sided tape attached to aluminium blocks affixed into the ToF-SIMS stage. For imaging studies 25 keV Bi^+ primary ions were used for analysis using a 256×256 pixel raster while ensuring the total ion fluence did not exceed the static limit. For surface sputtering the SIMS stage was rotated after acquisition using Bi^+ using the Eucentric capability of the Escosy stage control program (Raith, Dortmund, Germany), 10 keV C_{60}^+ primary ions were used to sputter a 1 mm area for 28 s then the stage was rotated again for analysis of the sputtered surface, this process was repeated four times. Microspheres were sectioned for ToF-SIMS analysis at Molecular Profiles Ltd. This was achieved using a Power Tome XL ultramicrotome (RMC, Boekeler Instruments, Tuscon, AZ) equipped with a diamond knife (DiATOME, Agar Scientific, Essex, UK). Microspheres were deposited on the surface of a light curable resin (Vitalit®, Eurobond Adhesives Ltd, Kent, UK), the resin was then cured immediately to prevent migration of resin into the microspheres.

Raman spectra were acquired using a WITec CRM200 (WITec Instruments Corp. Ulm, Germany) equipped with a 532 nm laser source, with the laser line suppressed by an edge filter. This laser excitation source was focused using a $100\times$ objective and the scattered light was collected using the same objective in an 180° backscatter regime. The Stokes shifted Raman scatter was dispersed using a 600 grooves/mm grating onto a Charged Coupled Device (CCD), providing a spectral resolution of $\sim 8\ \text{cm}^{-1}$.

Raman maps were acquired from between 20 and $30\ \mu\text{m}$ beneath the sample surface at intervals of $1\ \mu\text{m}$. Each Raman map was acquired over an area of $40\ \mu\text{m} \times 40\ \mu\text{m}$ and constructed using a serial mapping process. This involves the acquisition of spectra at defined points within an array using a CCD, and provides lateral and depth resolution of $\sim 1\ \mu\text{m}$. The spectra were not subjected to any spectral corrections to correct for aberrations or artefacts; however, the inherent signal from thermal noise was subtracted from each spectrum.

AFM was undertaken using a Veeco MultiMode AFM (Cambridge, UK), Quantitative Nanomechanical property Mapping (QNM) mode

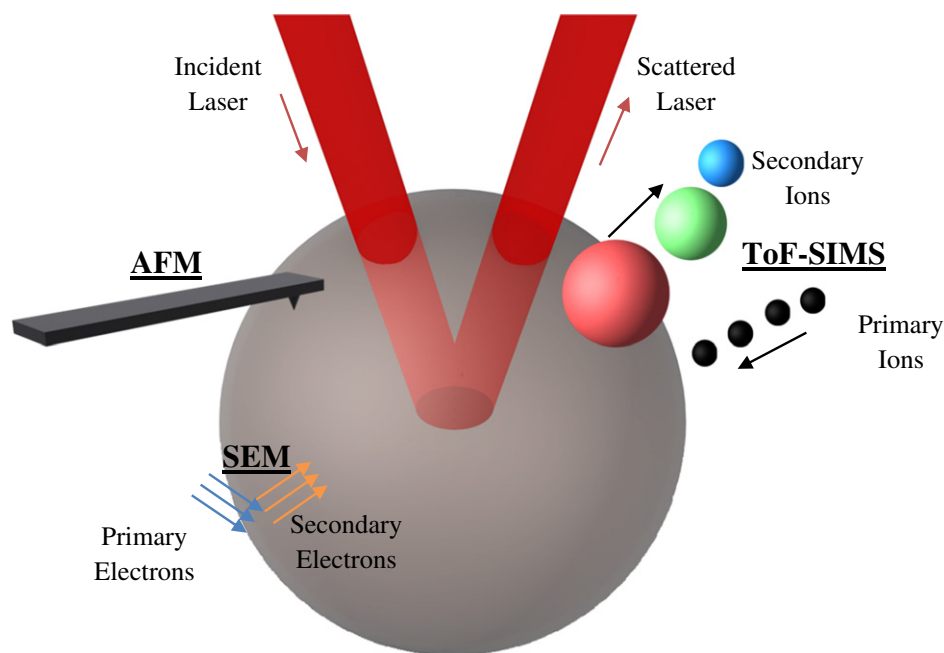


Fig. 1. Schematic diagram of analytical methods applied to the microsphere samples.

was used in order to provide maximal data from the scanning probe technique, as it allows for properties such as the Young's modulus (DMT model), adhesion and deformation to be measured while imaging at high resolution. An 8 μm area at the top of the microspheres were analysed before and after sputtering with C_{60}^{2+} primary ions.

JEOL JSM-6060LV scanning electron microscope (JEOL Ltd., Tokyo, Japan) was used, an acceleration voltage of 10 keV was used with no visible damage inflicted to the microsphere surfaces observed. Microspheres were prepared by sprinkling onto an adhesive carbon tab (12 mm wide) attached to an aluminum SEM stub (both from Agar Scientific, Essex, UK) which was then gently tapped on a piece of clean aluminum foil on a work bench to remove excess microspheres before being loaded into a Leica EM SCD050 gold coater (Leica Microsystems GmbH, Wetzlar, Germany) where they were coated for 2 min at 13 mA.

3. Results and discussion

SEM was employed to gain an understanding of the size distribution and surface topography of the lysozyme-PLGA microspheres (Fig. 2). The majority of microspheres appear smooth and spherical with their size varying between 30 and 150 μm in diameter, as shown in Fig. 2a. Fig. 2b shows at greater magnification the surface structure of some microspheres. We note pores at the surface of these microspheres ranging between 2 and 11 μm in size with a ring-like shallow depression morphology around some pores. Some circular, pitted surface structures were also found at the surface in the absence of a visible pore. There is no evidence of protein aggregates on the surface of the microspheres from SEM analysis [36].

The range of the particle size distribution was as expected from the process of w/o/w production of the microspheres [34] where a normal distribution of particle size is often observed. The surface pores observed are likely to be formed during the inversion stage of the microemulsion where the PVA water phase (which contains the protein) is encapsulated within the PLGA oil phase. Those water droplets that were not fully encapsulated and are at, or near the interface of the PLGA-rich oil droplets would be expected to produce the surface pores. The origin of the circular depressed surface features is

unknown but many such features as highlighted in Fig. 2b appear to be near to surface pores, suggesting that they may represent depressions formed by particularly thin wall sections.

An example of a negative ion ToF-SIMS spectrum of the PLGA lysozyme microspheres is shown in Fig. 3. After careful review of the ToF-SIMS analysis of the individual surfactant, polymer and protein controls and literature, diagnostic ions of each of the three components of the formulation may be distinguished in the ToF-SIMS analysis of the microspheres in Fig. 3. Peaks observed at m/z 71 and 73, and m/z 87 and 89 correspond to $[\text{M} \pm \text{H}]^-$ and $[\text{M} + \text{O} \pm \text{H}]^-$ respectively, where M is the repeat unit of LA monomer ($\text{C}_3\text{H}_4\text{O}_2$) of the PLGA copolymer [37]. The base peak (most prominent) of the spectrum at m/z 59 is diagnostic of PVA and corresponds to the acetate anion CH_3COO^- which has previously been used as a diagnostic peak in a PLGA/PVA system [15]. The high intensity of the acetate anion is derived from the unhydrolysed vinyl acetate monomers within the 87% hydrolysed PVA used in this study. For the lysozyme, the diagnostic peaks of CN^- and CNO^- at m/z 26 and 42 derived from the peptide sequence were selected as these can only arise from the protein in this formulation. In addition, multivariate curve resolution (data not shown) highlighted these peaks as being statistically significant and related specifically to the protein structure. The peaks selected were sufficiently intense to allow for the reconstruction of the spectra into an image format.

Using the diagnostic ions highlighted above, the ToF-SIMS spectra were reconstructed as images to characterise the distribution of the PLGA, PVA and lysozyme at the surface of the microspheres. Fig. 4 shows a ToF-SIMS image including a number of microspheres. Focusing on the main microsphere at the centre of the image, the ToF-SIMS image for PLGA is not continuous over the microsphere surface (Fig. 4a) indicating a discontinuous layer of PVA as illustrated in Fig. 4b where discrete features as small as 700 nm in diameter may be distinguished. The thickness of the PVA masks the underlying PLGA indicating that it is greater than the sampling depth of the ToF-SIMS of circa 1 nm under the static conditions employed in the ToF-SIMS analysis. Many of the features within the PVA film are circular and ring-like with many discrete isolated islands of the surfactant on the surface of the microsphere. Similar features are seen on the surface of the other smaller microspheres within Fig. 4b. At the apex of the central microsphere in Fig. 4, we observe a surface pore which is surrounded by an intense circular ring enriched in protein (Fig. 4c). Again, the thickness of this overlayer appears to be greater than 1 nm as no PLGA is detected in this region although there is evidence of the presence of PVA, particular on the outer portion of the ring structure and also as a discrete intense feature at the bottom lip of the pore. There is also lower intensity protein signals detected and associated with the PVA surfactant discontinuous layer (particularly visible in the lower left hand side of the main microparticle and also on other microparticle surfaces in Fig. 4c) but not on the bare PLGA surface. The overlay of all these three image sets in Fig. 4d clearly demonstrates the ability of ToF-SIMS to discriminate the different chemistries and their complex organisation on the microparticle surfaces. The original ToF-SIMS images from the instrument include a y-scale correction to account for the projection of the ion beam at an angle onto a planar sample. In these images, that modification is removed to accurately represent the dimensions of the particles as viewed from the ion source [38]. Thus, individual particles are accurately portrayed, but the distance between particles is compressed in the y direction.

Further representative ToF-SIMS images of microspheres ranging in size from 47 to 169 μm in diameter are demonstrated in Fig. 4e. All microspheres analysed again show a patchy discontinuous surfactant film at the surface of the microspheres and also the degree of coverage appears to be comparable between microspheres analysed. The surface lysozyme is again found primarily as highly intense circular ring-like structures surrounding near-surface pores.

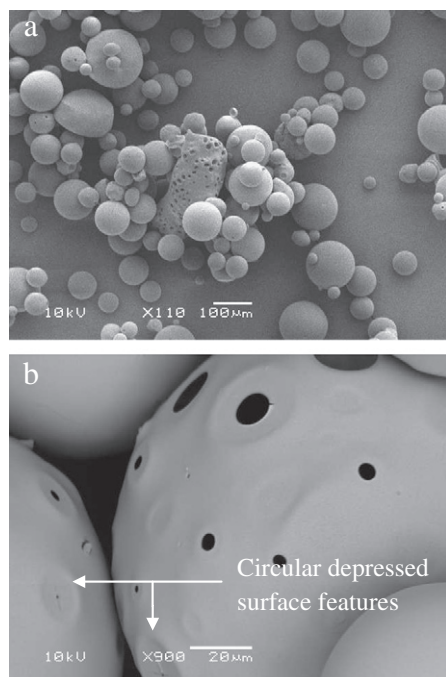


Fig. 2. SEM analysis of w/o/w lysozyme-PLGA microspheres.

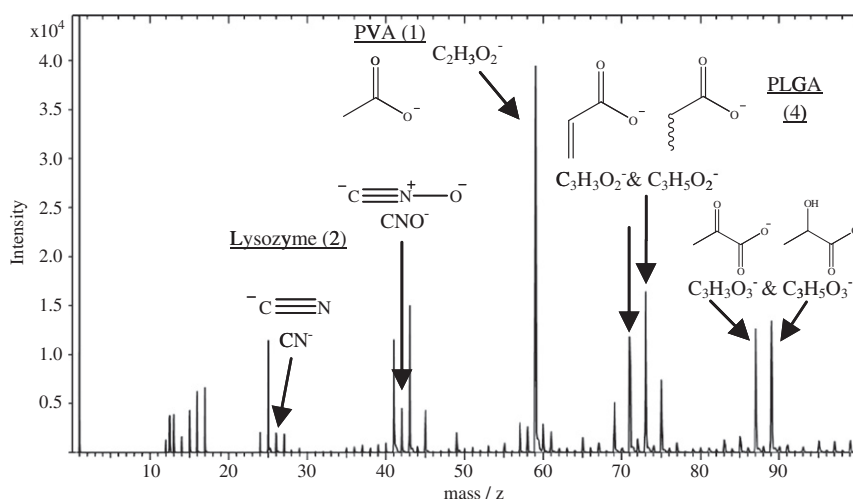


Fig. 3. Negative ToF-SIMS spectrum of the surface of PLGA lysozyme microspheres from a mass of 0 to 100, peaks used in the subsequent analysis are annotated (bracketed number indicates the number of unique ions used to represent each constituent).

ToF-SIMS sputtering and AFM analysis were applied to the surface of the microspheres in order to rationalise the thickness of the surfactant layer presented in Fig. 5. Fig. 5 a–d shows the surface of a microsphere which has been exposed to increasing sputtering with C_{60}^{2+} primary ions. The central microsphere focussed on measures 172 μm in diameter and is shown before sputtering in Fig. 5a. Two pores are clearly visible at the surface in addition to fissures, one pore appears empty and one rich in lysozyme. The characteristic discontinuous PVA layer is present at the surface and a diffuse distribution of lysozyme in regions rich with PVA is also observed, further suggesting a relationship between the spread of PVA and lysozyme at the surface. After the initial 28 s of sputtering shown in Fig. 5b, it is apparent the PVA surfactant layer is being eroded and is extremely thin, with much of it being removed from the right side of the image where sputtering is most effective revealing the PLGA substrate. The revealed PLGA surface confirms the presence of PVA as an overlayer at the surface of the microspheres and not a surface feature of the PLGA itself. The ion intensity of the diffuse surface lysozyme is also reduced and it is gradually apparent on sputtering that the origin of the surface lysozyme is related to the surface pores present (e.g. see pore which is labelled in Fig. 5b that was not clearly visible in Fig. 5a). On further sputtering shown in Fig. 5c and d, the PVA layer is removed and it is clear that one pore in particular is enriched with protein, however there is residual low intensity lysozyme signals from within other surface pores. It should be noted that a combination of spherical morphology of the microspheres and the primary ion beams being 180° from one another does not allow the sputtering to remove the PVA and lysozyme from the entire surface of the central microsphere (see upper top and left edge in Fig. 5). However the microsphere at the top left of the image has been effectively sputtered, which highlights topographical effects in ToF-SIMS imaging.

The secondary electron imaging of the ToF-SIMS, shown in Fig. 5e, illustrates the surface structures visible in the SIMS images and shows a thin fissure between three surface pores which was analysed with ToF-SIMS.

AFM images of the top of a microsphere before and after sputtering for 100 s are shown in Fig. 5f and g respectively. A thin smooth discontinuous overlayer was observed on all microspheres analysed before sputtering. Line analysis of the overlayer thickness across all data obtained showed an average overlayer thickness of 4.5 ± 0.8 nm. We note that Fig. 5f shows areas with a continuous film with the central region of random shaped island features which appear to have an equivalent height and form to the larger overlayer. After sputtering it is confirmed this layer is removed in its entirety and that it is preferentially sputtered leaving the rougher ($R_q = 3.01$ nm) PLGA visible.

In a previous work by Shard et al. on the sputtering of PLA, it was demonstrated that a C_{60} ion dose as applied in our work is consistent with 4 nm of PLA removed per sputtering cycle [39]. While this value may change depending on the polymeric material examined, it provides a useful benchmark for organic polymers. Interestingly, the thickness of 4.5 nm for the PVA layer determined by AFM correlates well with our sputtering data and also the work of Shard et al. In summary, the consistency of the overlayer thickness and the thickness of the smaller islands of discontinuous surfactant observed in Fig. 5f suggests a 4.5 nm thick PVA monolayer which remains after drying. A dynamic equilibrium model with PVA adsorbing and leaving the surface of the microspheres in the aqueous phase could explain the patchy morphology observed in the resultant microspheres [40].

Confocal Raman mapping was applied as a correlative technique for the ToF-SIMS analysis to provide a 3D understanding of the organisation of components across the surface and also within the bulk of the microspheres shown in Fig. 6. Confocal Raman analysis is feasible in this case due to the relative optical transparency of PLA. The confocal Raman map acquired from a single x–y plane in Fig. 6a shows the presence of pores ranging in size within the bulk of the microsphere. These are represented typically as black (indicating void space) or red (indicating lysozyme) spherical areas within the PLGA microsphere which is represented in green. These pores appear to range from 2 to 16 μm in diameter. The larger pores shown in Fig. 6a and b appear to be largely devoid of material within their centres. Conversely the smaller pore features at around 2 μm are filled with protein that consistently measure approximately 2 μm in diameter. This image is typical of all the microsphere structure observed. Such pores are formed during the inversion step of the double emulsion production method, however, the heterogeneous sizing, and distribution of protein within the pores suggests a complex mechanism is responsible for the distribution of components in the w/o/w system as shown by confocal Raman [41]. A protein coating is found adsorbed to the oil phase PLGA interface within some of the large pores. The thickness of this layer is variable as well as is the coverage. Fig. 6b provides an interpolated 3D representation generated using confocal Raman maps taken at 1 μm intervals in the z-axis and the 1 μm depth resolution allows for mathematical interpolation. This representation shows the protein distribution around a large pore which contains a significant concentration of protein adsorbed to the PLGA interface. We note that the small pores are found in close proximity to the larger pores. The images in Fig. 6a were created using 'Basis Analysis' [42] a multivariate approach whereby the spectra at each pixel are fit as a linear combination of 'basic' input spectra, in this case pure component spectra extracted from the images themselves shown in Fig. 6c.

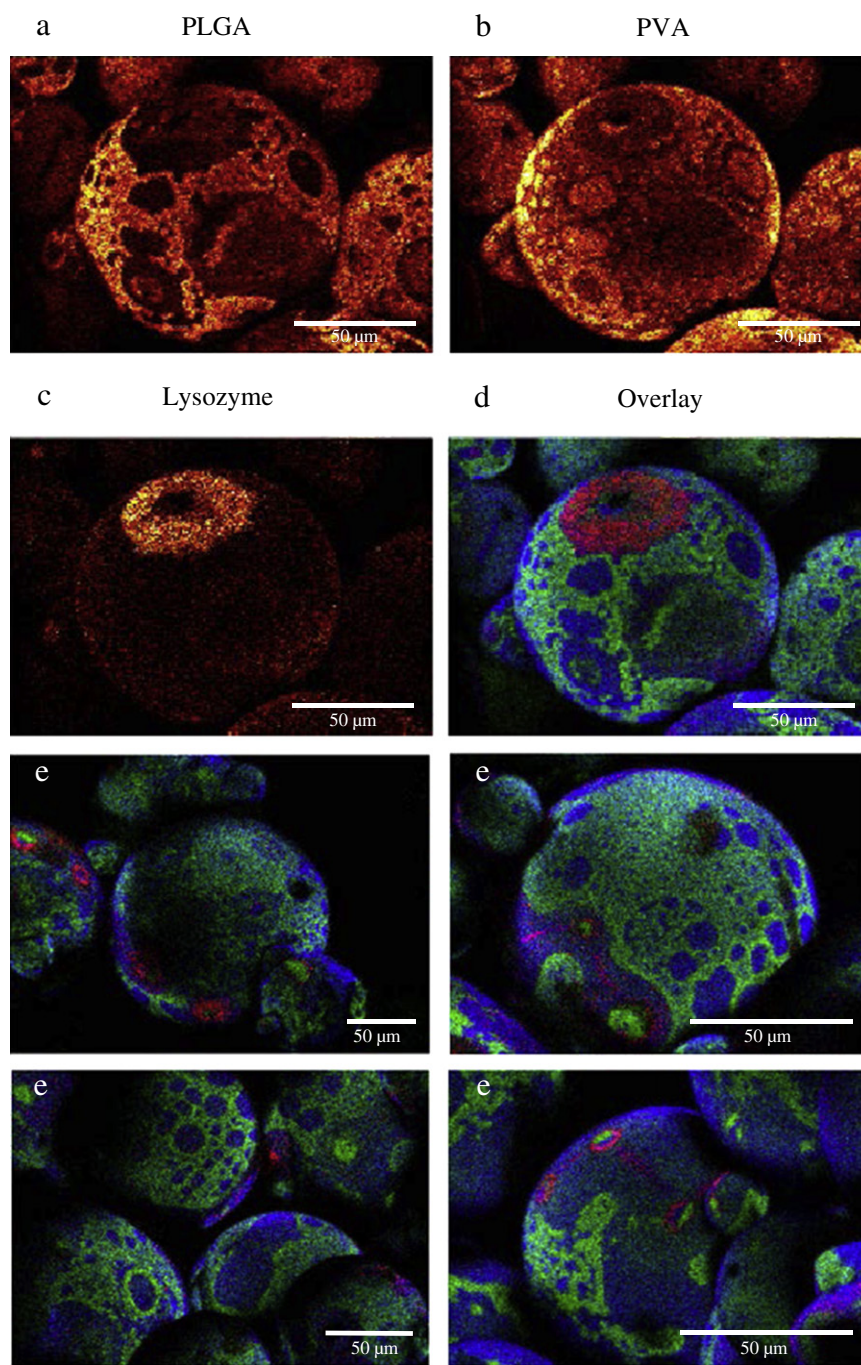


Fig. 4. ToF-SIMS imaging of the surface of a microsphere measuring 149 μm in diameter showing the secondary ion image generated from the diagnostic anions identified within the ToF-SIMS spectra, for a) PLGA (m/z 71/73 and 87/89), b) PVA (m/z 59), c) lysozyme (m/z 26 and 42) and d) an overlay showing PLGA (green), PVA (blue) and lysozyme (red). e) ToF-SIMS surface analysis of a range of w/o/w microspheres in overlay.

ToF-SIMS analysis of sectioned microspheres was undertaken to resolve the chemistry of the bulk of the microspheres (Fig. 7). Fig. 7c shows an overlay of lysozyme (red), PLGA (green) and PVA distribution (blue) in this cross section. We note pore features ranging in size from 2 μm to 18 μm in diameter which is comparable with the values determined by the confocal Raman analysis. Naturally, the maximum diameter of any pore feature may lie above or below the point of the cross section but both the confocal Raman and ToF-SIMS data illustrate the diversity in size and composition of the pores. When comparing Fig. 7a and b, lysozyme is clearly evident in some pores within the microsphere bulk. Again, it is present as dense cluster of protein in the smaller pore features and it appears

to cover the surface interface with the PLGA in some of the larger pores. The PVA visible as noted in Fig. 7c in one pore found in the bottom right of the image was a rare occurrence in our data suggesting that PVA does not remain in the bulk at significant a concentration. Alternatively a thin PVA layer could be stabilising the pores within the microsphere but due to the limitation of cross sectional analysis with ToF-SIMS imaging this layer may be difficult to observe.

ToF-SIMS cross-sectional analysis shows that many pores contain a large amount of lysozyme due to producing a 2D chemical representation of the 3D sample, in a way superimposing all protein within the depth of the pore. Confocal Raman analysis however confirms what is being imaged in the large pores is protein at the pore

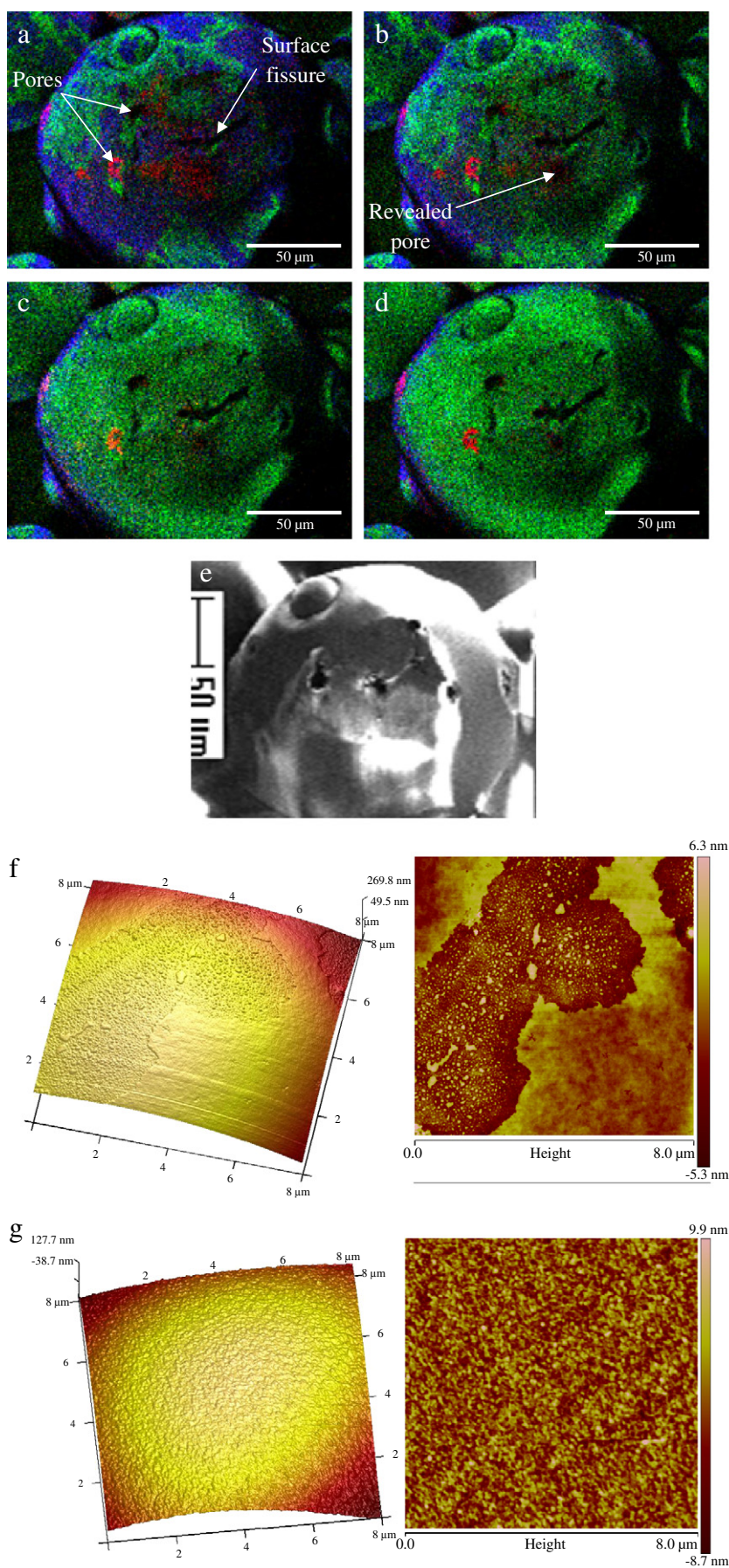


Fig. 5. a) ToF-SIMS of a microsphere before sputtering b) after 28 s, c) 56 s and d) 84 s of sputtering. e) Secondary electron image of the resulting microsphere. f) AFM height image of an 8 μm^2 area at the top of a microsphere before and g) after sputtering. Corresponding 3rd order flattened AFM height images are also shown.

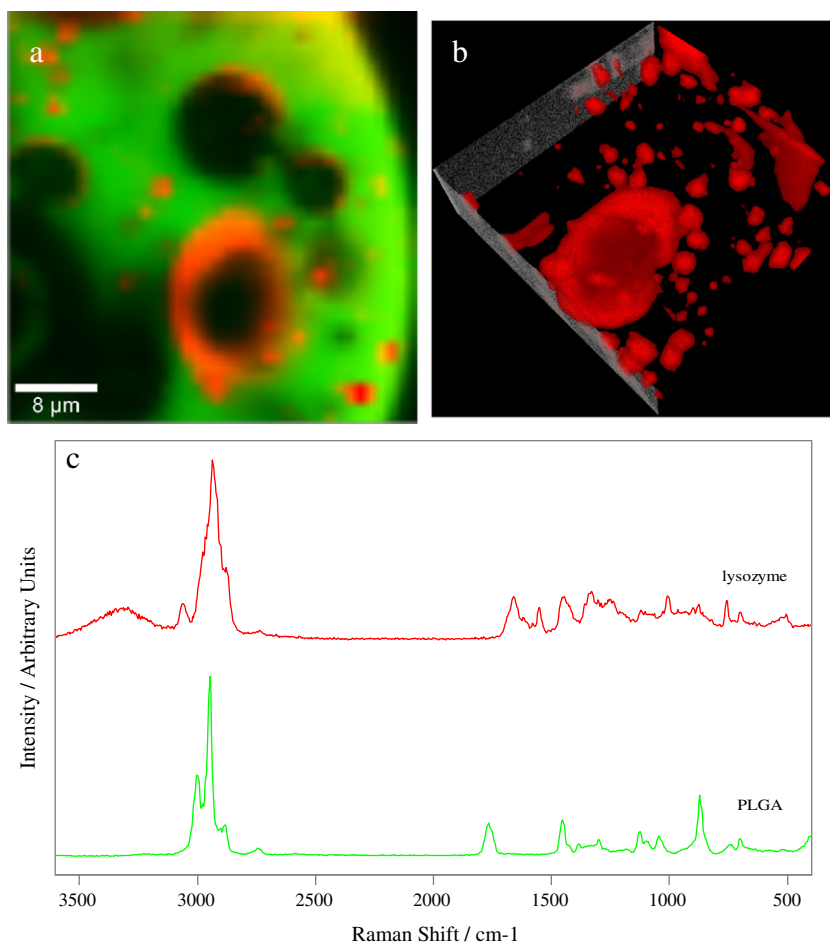


Fig. 6. a) A confocal Raman map indicating PLGA as green and lysozyme as red, showing large porous void spaces and protein adsorbed to the wall of the pore and small protein rich deposits measuring ~2 μm in diameter. b) An interpolated 3D representation of the protein distribution within a 40 × 40 × 10 μm volume of a microsphere showing from 20 μm into the microsphere surface (top of image) to 30 μm (bottom of image) of the microsphere bulk. c) Raman spectra between 3600 and 400 cm⁻¹ of lysozyme (red) and PLGA (green) extracted from the chemical maps and typical of the input spectra used to generate images such as that shown in Fig. 6a.

edges and base, illustrating the complimentary data generated from the high surface specificity and resolution of ToF-SIMS and the understanding of the 3D distribution of constituents achieved with confocal Raman mapping.

Our comprehensive analysis of the PLGA lysozyme system illustrates the potential for understanding the distribution of the protein and surfactant within the complex architecture of the microparticles formed from a multiple emulsion system. The visualisation of the surfactant layer on the surface of the microparticles is particularly notable. The ability of ToF-SIMS to detect the surfactant on a microparticle surface is dependent on the presence of intense diagnostic ion (at m/z 59) in the spectrum which is attributable only to the PVA. Present as a

discrete but laterally incomplete layer, ToF-SIMS and AFM were able to chemically and physically visualize respectively the integrity and pattern of the surfactant across the surface of the particles. The PLGA particles are formed in an excess of PVA and hence the detection of a complete homogenous PVA surface layer was initially expected. An effective PVA coating would be required to stabilize the microparticle formulation in solution and on evaporation of the organic solvent. Indeed, the surfactant concentration optimisation has an important role in reducing the diameter of the resulting microspheres through stabilisation of the emulsion droplets, reducing the occurrence of coalescence and allowing for a greater number of droplets to be encapsulated. A possible explanation of the incomplete

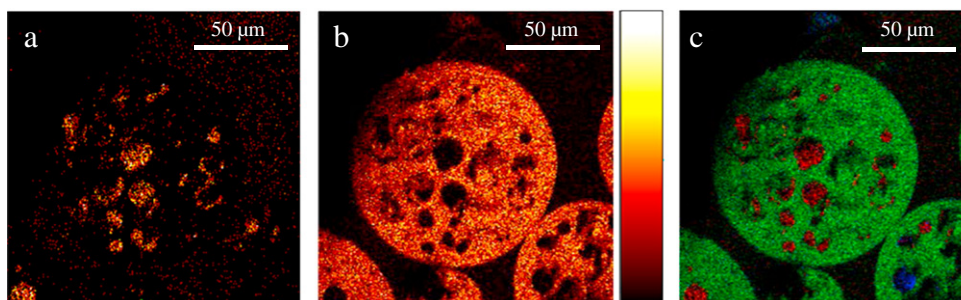


Fig. 7. ToF-SIMS of a sectioned microsphere showing a) lysozyme (CNO⁻), b) PLGA (C₃H₃O₂⁻, C₃H₅O₂⁻, C₃H₃O₃⁻ & C₃H₅O₃⁻), and c) an overlay showing lysozyme (red), PLGA (green) and PVA (C₂H₃O₂⁻ blue).

lateral PVA coverage on the microparticle surface may be due to the contraction of the film during the rinsing and drying process, leaving an incomplete PVA layer of surprisingly uniform thickness.

Our studies show that the protein on the surface of the microparticles is organised in a number of ways: firstly, the majority of the surface protein appears to be densely clustered around features that are associated with sub-surface protein filled pores that intersect the outer surface of the microparticles. This suggests incomplete encapsulation of the protein rich water droplets in the particle formation process. Secondly, there is evidence for the presence of protein dispersed within the surfactant film layer itself. The mechanism responsible for this may be related to the ionic interaction between the protein and PVA in addition to surface segregation often observed with proteins on biomaterials [43]. This work represents the first example where the spatial location of the protein, surfactant and the polymer substrate in the ToF-SIMS images of the microparticle surfaces has been demonstrated.

With regard to the bulk distribution of the protein within the microparticles, confocal Raman analysis of the intact particles and the ToF-SIMS imaging of the microtomed particles confirm that lysozyme is located in the pores formed by the evaporation of water from the aqueous droplets dispersed within the PLA rich organic phase. The wide size distribution of these pores suggests incomplete stabilisation of the water droplets by the PVA surfactant, the larger ones potentially being formed via coalescence of the droplets during the removal of solvent during the particle production process. The internal contents of microemulsion droplets are known to diffuse and undergo collisions. If these collisions are sufficiently energetic the surfactant film may rupture causing droplet exchange which may explain the size distribution [44]. Both the Raman and ToF-SIMS analysis show the presence of a population of smaller pores (2–5 μm) which are protein rich dispersed throughout the microparticles. In contrast, protein only coats the inner surface of the larger pores (up to 20 μm) leaving the majority of the volume unoccupied. The mechanism for the formation of such void spaces is unclear in the latter case but the potential coalescence of protein rich water droplets during the particle production may play a role as the subsequent removal of water at the droplet interface would promote the transport of the protein with this solvent front to the surface of the pore. Due to the charged domains found on proteins, ionic interactions with the negatively charged PVA may explain the crucial nature of protein and PVA interaction in the distribution of protein throughout the microspheres [45]. Surface segregation will also be influenced by the hydrophobic effect which influences lysozyme aggregation and folding in aqueous environments due to all non-covalent bonding being affected by the folding of protein in solution [46]. Our analysis has revealed a complex and heterogeneous organisation of protein distribution within the microparticle bulk that may have an impact on the mechanism and kinetics of release of the protein from such systems [43].

4. Conclusions

Partially porous protein loaded microspheres for use as controlled drug delivery biomaterials have had their surface and bulk scrutinised with complimentary analytical techniques. For the first time we have shown the ability to spatially image surfactant PVA and protein adsorbed to the surface of microspheres using ToF-SIMS imaging. The surfactant layer has a thickness of circa 4 nm and can be removed under ToF-SIMS sputtering studies which is confirmed by AFM. The ability to spatially map the surface and bulk microparticles prepared by the double emulsion approach has revealed that distribution of the lysozyme to be complex and heterogeneous. We believe the combined approach of using the analytical techniques of ToF-SIMS (imaging and sputtering), confocal Raman, AFM and other complimentary methodologies provides a powerful toolset for the study of the spatial chemical distribution of biomolecules and excipients

such as surfactants within controlled release formulations, for instance microparticles. They have been shown to be highly complementary techniques for the characterisation of controlled release injectables and by association, implantable formulations, increasing our understanding of influence of the fabrication process and formulation composition on the properties of the resulting delivery systems.

Acknowledgements

We would like to thank the BBSRC, NPL and Wellcome Trust award 085246/Z/08/Z for their funding and Molecular Profiles Ltd. for their expertise and use of their Raman spectrometer and ultramicrotome.

References

- [1] A. Grenha, B. Seijo, C. Serra, C. Remunan-Lopez, Chitosan nanoparticle-loaded mannitol microspheres: structure and surface characterization, *Biomacromolecules* 8 (2007) 2072–2079.
- [2] J. Chesko, J. Kazzaz, M. Ugozzoli, M. Singh, D.T. O'Hagan, C. Madden, M. Perkins, N. Patel, Characterization of antigens adsorbed to anionic PLG microparticles by XPS and TOF-SIMS, *Indian J. Pharm. Sci.* 97 (2008) 1443–1453.
- [3] C.Y. Dai, B.C. Wang, H.W. Zhao, Microencapsulation peptide and protein drugs delivery system, *Colloids Surf. B Biointerfaces* 41 (2005) 117–120.
- [4] M. Koneracka, M. Muckova, V. Zavisova, N. Tomasovicova, P. Kopcansky, M. Timko, A. Jurikova, K. Csach, V. Kavecansky, G. Lancz, Encapsulation of anticancer drug and magnetic particles in biodegradable polymer nanospheres, *J. Phys. Condens. Matter* 20 (2008).
- [5] A. Grenha, B. Seijo, C. Remuñán-López, Microencapsulated chitosan nanoparticles for lung protein delivery, *Eur. J. Pharm. Sci.* 25 (2005) 427–437.
- [6] Y. Men, C. Thomasin, H.P. Merkle, B. Gander, G. Corradin, A single administration of tetanus toxoid in biodegradable microspheres elicits T-cell and antibody-responses similar or superior to those obtained with aluminum hydroxide, *Vaccine* 13 (1995) 683–689.
- [7] M. Singh, M. Briones, G. Ott, D. O'Hagan, Cationic microparticles: a potent delivery system for DNA vaccines, *Proc. Natl. Acad. Sci. U. S. A.* 97 (2000) 811–816.
- [8] D. O'Hagan, M. Singh, M. Ugozzoli, C. Wild, S. Barnett, M.C. Chen, M. Schaefer, B. Doe, G.R. Otten, J.B. Ulmer, Induction of potent immune responses by cationic microparticles with adsorbed human immunodeficiency virus DNA vaccines, *J. Virol.* 75 (2001) 9037–9043.
- [9] H. Okada, One- and three-month release injectable microspheres of the LH-RH superagonist leuporelin acetate, *Adv. Drug Deliv. Rev.* 28 (1997) 43–70.
- [10] M. Bolla, D. Gonzalez, P. Warde, J.B. Dubois, R.O. Mirimanoff, G. Storme, J. Bernier, A. Kuten, C. Sternberg, T. Gil, L. Collette, M. Pierart, Improved survival in patients with locally advanced prostate cancer treated with radiotherapy and goserelin, *N. Engl. J. Med.* 337 (1997) 295–300.
- [11] T. Kotake, M. Usami, H. Akaza, K. Koiso, Y. Homtna, K. Kawabe, Y. Aso, S. Orikasa, J. Shimazaki, S. Isaka, O. Yoshida, Y. Hirao, E. Okajima, S. Naito, J. Kumazawa, H. Kanetake, Y. Saito, Y. Ohi, Y. Ohashi, Z.S. Group, Goserelin acetate with or without antiandrogen or estrogen in the treatment of patients with advanced prostate cancer: a multicenter, randomized, controlled trial in Japan, *Jpn. J. Clin. Oncol.* 29 (1999) 562–570.
- [12] S.F. Kemp, P.J. Fielder, K.M. Attie, S.L. Blethen, E.O. Reiter, K.M. Ford, M. Marian, L.N. Dao, H.J. Lee, P. Saenger, Pharmacokinetic and pharmacodynamic characteristics of a long-acting growth hormone (GH) preparation (nutropin depot) in GH-deficient children, *J. Clin. Endocrinol. Metab.* 89 (2004) 3234–3240.
- [13] V.R. Sinha, A. Trehan, Biodegradable microspheres for parenteral delivery, *Crit. Rev. Ther. Drug Carrier Syst.* 22 (2005) 535–602.
- [14] M.C. Davies, A. Brown, J.M. Newton, S.R. Chapman, SSIMS and SIMS imaging analysis of a drug delivery system, *Surf. Interface Anal.* 11 (1988) 591–595.
- [15] P.D. Scholes, A.G.A. Coombes, L. Illum, S.S. Davis, J.F. Watts, C. Ustariz, M. Vert, M.C. Davies, Detection and determination of surface levels of poloxamer and PVA surfactant on biodegradable nanospheres using SSIMS and XPS, *J. Control. Release* 59 (1999) 261–278.
- [16] A.M. Belu, M.C. Davies, J.M. Newton, N. Patel, TOF-SIMS characterization and imaging of controlled-release drug delivery systems, *Anal. Chem.* 72 (2000) 5625–5638.
- [17] C.M. Mahoney, D.V. Patwardhan, M.K. McDermott, Characterization of drug-eluting stent (DES) materials with cluster secondary ion mass spectrometry (SIMS), *Appl. Surf. Sci.* 252 (2006) 6554–6557.
- [18] A. Belu, C. Mahoney, K. Wormuth, Chemical imaging of drug eluting coatings: combining surface analysis and confocal Raman microscopy, *J. Control. Release* 126 (2008) 111–121.
- [19] G.L. Fisher, A.M. Belu, C.M. Mahoney, K. Wormuth, N. Sanada, Three-dimensional time-of-flight secondary ion mass spectrometry imaging of a pharmaceutical in a coronary stent coating as a function of elution time, *Anal. Chem.* 81 (2009) 9930–9940.
- [20] K.M. Shakesheff, M.C. Davies, D.E. Jackson, C.J. Roberts, S.J.B. Tendler, V.A. Brown, R.C. Watson, D.A. Barrett, P.N. Shaw, Imaging the surface of silica microparticles with the atomic-force microscope – a novel sample preparation method, *Surf. Sci.* 304 (1994) L393–L399.

- [21] L. Mu, S.S. Feng, Fabrication, characterisation and in vitro release of paclitaxel (Taxol) loaded poly (lactic-co-glycolic acid) microspheres prepared by spray drying technique with lipid/cholesterol emulsifiers, *J. Control. Release* 76 (2001) 239–254.
- [22] C.M. Yang, D. Plackett, D. Needham, H.M. Burt, PLGA and PHBV microsphere formulations and solid-state characterization: possible implications for local delivery of fusidic acid for the treatment and prevention of orthopaedic infections, *Pharm. Res.* 26 (2009) 1644–1656.
- [23] H.J. van Manen, A.A. van Apeldoorn, R. Verrijck, C.A. van Blitterswijk, C. Otto, Intracellular degradation of microspheres based on cross-linked dextran hydrogels or amphiphilic block copolymers: a comparative Raman microscopy study, *Int. J. Nanomedicine* 2 (2007) 241–252.
- [24] K.M. Balss, G. Lianos, G. Papandreou, C.A. Maryanoff, Quantitative spatial distribution of sirolimus and polymers in drug-eluting stents using confocal Raman microscopy, *J. Biomed. Mater. Res. A* 85A (2008) 258–270.
- [25] E. Kang, J. Robinson, K. Park, J.-X. Cheng, Paclitaxel distribution in poly(ethylene glycol)/poly(lactide-co-glycolic acid) blends and its release visualized by coherent anti-Stokes Raman scattering microscopy, *J. Control. Release* 122 (2007) 261–268.
- [26] R. Szostak, S. Mazurek, Quantitative determination of acetylsalicylic acid and acetaminophen in tablets by FT-Raman spectroscopy, *Analyst* 127 (2002) 144–148.
- [27] S. Mazurek, R. Szostak, Quantitative determination of diclofenac sodium in solid dosage forms by FT-Raman spectroscopy, *J. Pharm. Biomed. Anal.* 48 (2008) 814–821.
- [28] S. Sasic, D.A. Clark, J.C. Mitchell, M.J. Snowden, A comparison of Raman chemical images produced by univariate and multivariate data processing—a simulation with an example from pharmaceutical practice, *Analyst* 129 (2004) 1001–1007.
- [29] L. Zhang, M.J. Henson, S.S. Sekulic, Multivariate data analysis for Raman imaging of a model pharmaceutical tablet, *Anal. Chim. Acta* 545 (2005) 262–278.
- [30] M.J. Whitaker, R.A. Quirk, S.M. Howdle, K.M. Shakesheff, Growth factor release from tissue engineering scaffolds, *J. Pharm. Pharmacol.* 53 (2001) 1427–1437.
- [31] Q.P. Hou, P.A. De Bank, K.M. Shakesheff, Injectable scaffolds for tissue regeneration, *J. Mater. Chem.* 14 (2004) 1915–1923.
- [32] D.H.R. Kempen, L. Lu, T.E. Hefferan, L.B. Creemers, A. Maran, K.L. Classic, W.J.A. Dhert, M.J. Yaszemski, Retention of in vitro and in vivo BMP-2 bioactivities in sustained delivery vehicles for bone tissue engineering, *Biomaterials* 29 (2008) 3245–3252.
- [33] S. Cohen, T. Yoshioka, M. Lucarelli, L.H. Hwang, R. Langer, Controlled delivery systems for proteins based on poly(lactic glycolic acid) microspheres, *Pharm. Res.* 8 (1991) 713–720.
- [34] S. Ravi, K.K. Peh, Y. Darwis, B.K. Murthy, T.R.R. Singh, C. Mallikarjun, Development and characterization of polymeric microspheres for controlled release protein loaded drug delivery system, *Indian J. Pharm. Sci.* 70 (2008) 303–309.
- [35] A. Rafati, M.C. Davies, A.G. Shard, S. Hutton, G. Mishra, M.R. Alexander, Quantitative XPS depth profiling of codeine loaded poly(L-lactic acid) films using a coronene ion sputter source, *J. Control. Release* 138 (2009) 40–44.
- [36] K. Park, J.S. Park, D.G. Woo, H.N. Yang, H.-M. Chung, K.-H. Park, The use of chondrogenic differentiation drugs to induce stem cell differentiation using double bead microsphere structure, *Biomaterials* 29 (2008) 2490–2500.
- [37] A.G. Shard, M.C. Davies, Y.X. Li, C. Volland, T. Kissel, XPS and SSIMS analysis revealing surface segregation and short-range order in solid films of block copolymers of PEO and PLGA, *Macromolecules* 30 (1997) 3051–3057.
- [38] S. Rangarajan, B.J. Tyler, Topography in secondary ion mass spectroscopy images, *J. Vac. Sci. Technol., A* 24 (2006) 1730.
- [39] A.G. Shard, P.J. Brewer, F.M. Green, I.S. Gilmore, Measurement of sputtering yields and damage in C60SIMS depth profiling of model organic materials, *Surf. Interface Anal.* 39 (2007) 294–298.
- [40] S.N. Moorkanikara, D. Blankschtein, New methodology to determine equilibrium surfactant adsorption properties from experimental dynamic surface tension data, *Langmuir* 25 (2009) 6191–6202.
- [41] M.R. Bohmer, J.A.M. Steenbakkers, C. Chlon, Monodisperse polymeric particles prepared by ink-jet printing: double emulsions, hydrogels and polymer mixtures, *Colloids Surf. B Biointerfaces* 79 (2010) 47–52.
- [42] U. Schmidt, S. Hild, O. Hollricher, Characterization of Thin Polymer Films on the Nanometer Scale with Confocal Raman AFM, *Macromolecular Symposia*, 2005.
- [43] K. Fu, R. Harrell, K. Zinski, C. Um, A. Jaklenec, J. Frazier, N. Lotan, P. Burke, A.M. Klibanov, R. Langer, A potential approach for decreasing the burst effect of protein from PLGA microspheres, *J. Pharm. Sci.* 92 (2003) 1582–1591.
- [44] P.D.I. Fletcher, A.M. Howe, B.H. Robinson, The kinetics of solubilisation exchange between water droplets of a water-in-oil microemulsion, *J. Chem. Soc., Faraday Trans. 1* 83 (1987) 985–1006.
- [45] C.A. Haynes, W. Norde, Structures and stabilities of adsorbed proteins, *J. Colloid Interface Sci.* 169 (1995) 313–328.
- [46] W. Kauzmann, Some factors in the interpretation of protein denaturation, *Adv. Protein Chem.* 14 (1959) 1–63.